Feasibility study of time-lapse seismic monitoring of CO_2 sequestration.

Marie Macquet, Don C. Lawton, Jessica Dongas and Jacky Barraza

ABSTRACT

Geological sequestration is one way to reduce our CO_2 emissions in the atmosphere. Background studies are made prior to the beginning of the injection to ensure the security of this method. In the CaMI.FRS project near Brooks, Alberta, numerous wells give us information about the lithology, the porosity, the permeability, the velocities (and many others parameters) of the medium. Beside these direct data, seismic studies were conducted in order to characterize the subsurface.

After this prior work is done, numerical simulations were done in order to characterize the feasibility of the time-lapse seismic monitoring. Indeed, once the injection begins, seismic survey will be made at regular intervals to monitor the CO_2 injection. Fluid simulations allow us to work on synthetic models, but yet are close to what we expect in the reality.

We use here Gassmann fluid substitution to obtain the elastic parameters (V_P, V_S and ρ) for different time of injection (1 year after the beginning of the injection and 1 year after the end of the injection), for a $300m$ depth CO_2 reservoir. In those models, synthetic data are generated then processed. This work give us a good approximation of the feasibility of a time-lapse seismic monitoring, considering the conditions of CaMI.FRS project.

INTRODUCTION

The Containment and Monitoring Institute (CaMI) is a part of CMC Research Institutes Inc (CMC). In collaboration with the University of Calgary, they developed the Field Research Station (FRS) in Newell County, Alberta, near Brooks. The goal of the CaMI.FRS is to develop research and improvement for containment and storage of CO_2 (see for example Lawton et al. (2015b)). One of the main focus of CaMI.FRS is the MMV (Monitoring, Measurement and Verification) of the CO_2 sequestration. The plan is to inject small amount of gas (around 1000 tons/year over 5 years) at $300m$ and $500m$ depth. This controlled release of CO_2 will allow us, for example, to develop improved monitoring technologies on a small amount of CO_2 injected at shallow depth.

The principle of monitoring injection of CO_2 is to acquire surveys at different times during the injection in order to track the changes in the medium. We need a baseline, acquired before the injection, which will serve in the future as reference for the monitoring. Several surveys were already acquired in the CaMI.FRS, including in the last past years a 3C-3D seismic survey in 2014 (Lawton et al., 2015a), 3C-2D surface seismic and walkaway VSP experiment (Hall et al., 2015). Those surveys, in addition to characterizing the injection site, will serve as the baseline for future monitoring studies.

Before starting the CO_2 injection, we can already work on the feasibility of seismic monitoring using synthetic data. This is the purpose of the work presented here. First, we

present the Gassmann fluid substitution we used to generate the different models (V_P, V_S and ρ) and discuss the results. An important part is the presentation of the input data. Indeed, accurate input data give an accurate and validated modelling, and particular attention was to produce models the most faithful to the reality. In a second time, we focus on the data simulation and the processing, and discuss the results. Last, we discuss on the work currently in progress as well as the planed future work.

The plan at CaMI.FRS is to inject CO_2 over a period of 5 years. Figure 1 shows the extend of the expected CO_2 plume after 1 year (green) and 6 years (red) of injection for the $300m$ depth reservoir. During this work, we focussed on these two periods :

- 1 year after the beginning of the injection, called also t = 1 year (see green line on Figure 1).
- 1 year after the end of the injection, called also t = 6 years (see red line on Figure 1).

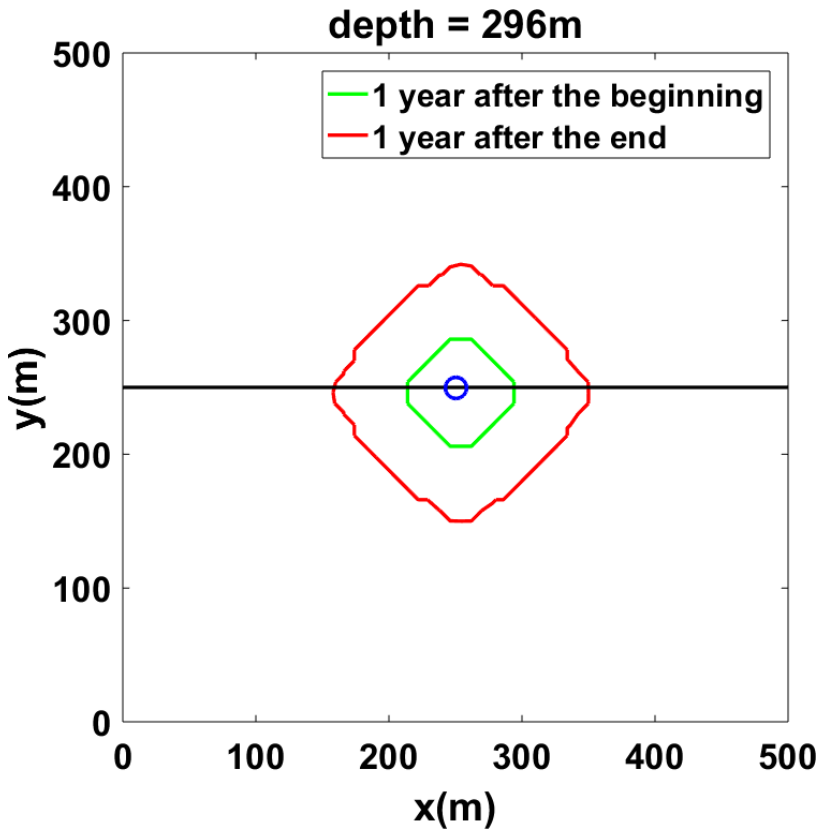

FIG. 1. Horizontal sections (at depth = 296m) of the maximum extension of the CO_2 injection plume, 1 year after the beginning of the injection (in green) and 1year after the end of the injection (in red). In this report, 2D sections are plotted for y=250m (black line) and 1D profiles are located along the injection well at $x = y$ =250m (blue circle). Modified from Barraza (2016).

FLUID SUBSTITUTION

Theory

Gassmann's equation (Gassmann (1951) and its English translation Gassmann (1998)) are here used to simulate the fluid substitution for the time-lapse monitoring study. Gassmann's equation links the bulk modulus of a rock to its pore, frame and fluid properties by the equation 1.

$$K_{sat} = K^* + \frac{1 - (\frac{K^*}{K_0})^2}{\frac{\phi}{K_{fl}} + \frac{(1-\phi)}{K_0} - \frac{K^*}{K_0^2}} \tag{1}$$

where K_{sat} is the saturated bulk modulus ; K^* the frame bulk modulus (or bulk modulus of the porous rock frame, drained of any pore-filling fluid) ; K_0 the bulk modulus of the mineral matrix ; ϕ the porosity and K_{fl} the bulk modulus of the fluid.

We present here an overview of the steps used for the Gassmann fluid substitution.

Step 1. We calculated the initial saturated bulk modulus and the initial shear modulus using the initial elastic parameters (equations 2 and 3).

$$K_{sat_{init}} = \rho_{init}(V_{P_{init}}^2 - \frac{4}{3}V_{S_{init}}^2) \tag{2}$$

$$\mu_{init} = \rho_{init}V_{S_{init}}^2 \tag{3}$$

where $V_{P_{init}}$, $V_{S_{init}}$ and ρ_{init} are the initial elastic parameters (of the baseline model).

Note that the shear modulus remains constant during your fluid substitution, so $\mu_{init} = \mu_{sat}$.

Step 2. We need to know the bulk modulus and the density of the fluid at the initial stage and after the CO_2 injection (called $K_{fl_{init}}$, $K_{fl_{new}}$, $\rho_{fl_{init}}$ and $\rho_{fl_{new}}$). They are calculated using equations 4 and 5.

$$\rho_{fl} = \sum_{i=1}^{n} S_i\rho_i \tag{4}$$

$$K_{fl} = [\sum_{i=1}^{n} \frac{S_i}{K_i}]^{-1} \tag{5}$$

where S_i is the saturation of the i^{th} individual phase which composes the fluid ; ρ_i and K_i are the associated density and the bulk modulus. Here, the two different component which constitute the fluid are the brine and the CO_2.

$$K_{fl} = [\frac{S_{brine}}{K_{brine}} + \frac{S_{CO_2}}{K_{CO_2}}]^{-1} \tag{6}$$

$$\rho_{fl} = S_{brine} * \rho_{brine} + S_{CO_2} * \rho_{CO_2} \tag{7}$$

where ρ_{brine}, ρ_{CO_2}, K_{brine} and K_{CO_2} are calculated using the equations of Batzle and Wang (1992). They are dependant of the salinity, temperature and the pressure (and intrinsically of the depth). Table 1 resumes the average values obtained for this study.

Table 1. Bulk modulus and density for brine, CO_2 and fluid composed of 30% of CO_2 for P and T reservoir conditions.

	t = 1 year		t = 6 years	
	$K(GPa)$	$\rho(g.cc^{-1})$	$K(GPa)$	$\rho(g.cc^{-1})$
brine = initial fluid	2.14	1.002	2.14	1.002
CO_2	0.005	0.083	0.004	0.067
new fluid (for 30% CO_2 sat.)	0.026	0.82	0.013	0.69

Step 3. Here, we calculate the frame bulk modulus (equation 8). We need to know the matrix bulk modulus (K_0) and the initial fluid bulk modulus ($K_{fl_{init}}$). Initial fluid bulk modulus is equal to the brine bulk modulus because the CO_2 saturation is equal to 0% in the initial model.

$$K^* = \frac{K_{sat}(\frac{\phi K_0}{K_{fl_{init}}} + 1 - \phi) - K_0}{\frac{\phi K_0}{K_{fl_{init}}} + \frac{K_{sat}}{K_0} - 1 - \phi} \tag{8}$$

The matrix bulk modulus K_0 is calculated using equation 9. This parameter depend of the minerals which composed the matrix and the bulk modulus associated to each minerals. K_0 remains constant with the fluid substitution.

$$K_0 = \frac{1}{2}[K_{Reuss} + K_{Voigt}] \tag{9}$$

where K_{Reuss} and K_{Voigt} are calculated using equations 10 and 11.

$$K_{Reuss} = [\sum_{i=1}^{n} \frac{V_i}{K_i}]^{-1} \tag{10}$$

$$K_{Voigt} = \sum_{i=1}^{n} V_i K_i \tag{11}$$

where V_i is the volumetric fraction of the i^{th} mineral which composes the matrix and K_i is the associated bulk modulus.

Step 4. The new saturated bulk modulus is calculated using the new fluid bulk modulus (equation 12).

$$K_{sat_{new}} = K^* + \frac{[1 - (\frac{K^*}{K_0})]^2}{\frac{\phi}{K_{fl_{new}}} + \frac{(1-\phi)}{K_0} - \frac{K^*}{K_0^2}} \tag{12}$$

Step 5. Finally, we calculate the new elastic parameters using equations 13-15.

$$\rho_{new} = \rho_{matrix}(1 - \phi) + \rho_{fl_{new}}\phi \tag{13}$$

$$V_{P_{new}} = \sqrt{\frac{K_{sat_{new}} + \frac{4}{3}\mu_{sat}}{\rho_{new}}} \tag{14}$$

$$V_{S_{new}} = \sqrt{\frac{\mu_{sat}}{\rho_{new}}} \tag{15}$$

Input data

An important effort was made to use the most accurate input data to have a fluid substitution that is most faithful to reality.

First, we need to know the initial elastic parameters. We use the V_P, ρ and V_P/V_S logs from the injection well. We consider a layer-cake model, which means that the model is laterally homogeneous. The initial parameters are shown on Figure 2.

We use the geostatic model provided by Dongas (2016) and upgraded by Barraza (2016). Numerous wells located around the CaMI.FRS give very accurate information about the parameters of the rocks. As wells give local information, they need to be extrapolated (with the help of 3D seismic data) to build a 3-D geostatic model of the porosity and the permeability. A dynamic fluid flow simulation was made from the geostatic model to estimate the CO_2 saturation and the pressure in the reservoir (Figures 3 and 4). The parameters used in this study are the porosity from the geostatic model (ϕ), the CO_2 concentration and the pressure.

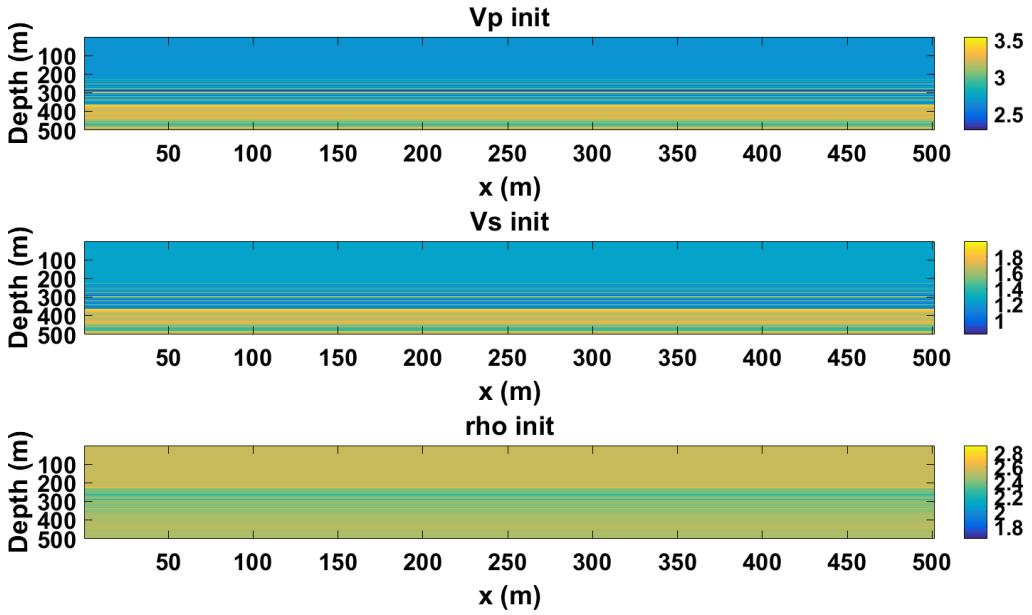

FIG. 2. Initial parameters used for Gassmann fluid substitution. Top : P-wave velocity ($km.s^{-1}$) ; middle : S-wave velocity ($km.s^{-1}$) ; bottom : density ($g.cm^{-3}$).

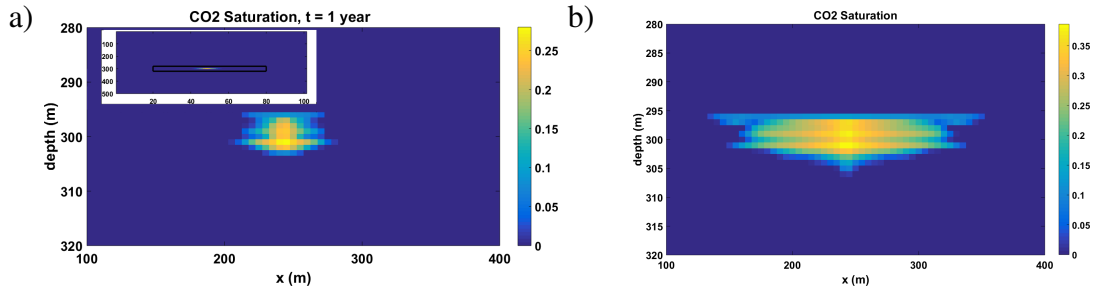

FIG. 3. a) CO_2 saturation from Barraza (2016), 1 year after the beginning of the injection, focussed on the reservoir injection. Insert in this figure is the entire model. b) CO_2 saturation from Barraza (2016), 1 year after the end of the injection, focussed on the reservoir injection.

Figure 4 also shows the profiles for the temperature and the pressure in our models. We use a linear gradient of $23.5°C.km^{-1}$ for the temperature, with a temperature at the surface of $5°C$. Note on Figure 4 that the pressure inside the reservoir decreases with time. Indeed, at t = 6 years, we are 1 year after the end of the injection, and the pressure becomes reduced because of diffusion.

The CO_2 concentration and the pressure were modelled for different times, during the injection phase and after the end of the injection (see Dongas (2016)). In this study, we focussed on two times, 1 year after the beginning of the injection and 1 year after the end of the injection (called t = 1 year and t = 6 years respectively).

Figure 5 shows the mineral composition coming from the ELAN logs (Schlumberger, CMC), focussed on the interest zone. The proportion of each mineral which composed the matrix allow us to calculate an accurate matrix bulk modulus (K_0, equation 9). The well logs are 1D measurement, nevertheless, as we estimate our model as a layer-cake model, the 1D profiles can be extrapolated as a 3D model.

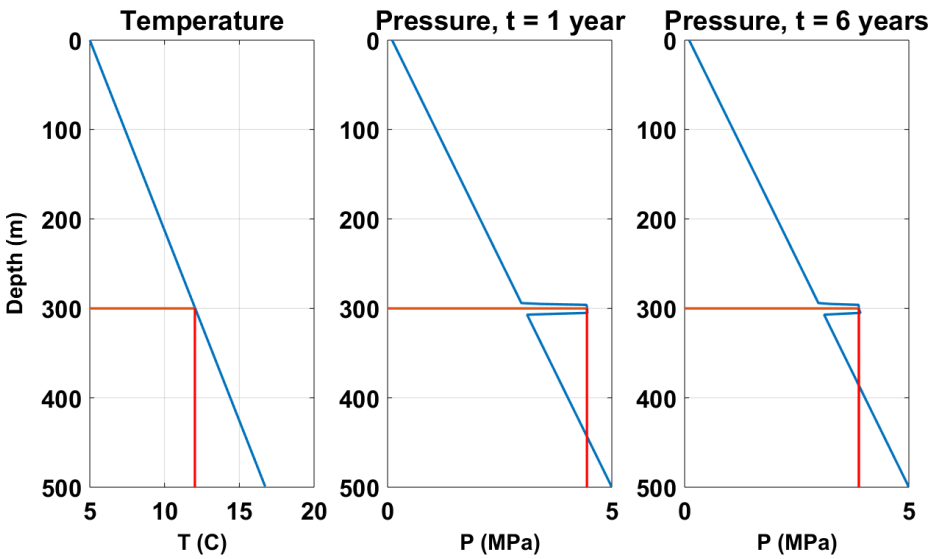

FIG. 4. Left: Temperature profile (same for t = 1 year and t = 6 years) ; middle: Pressure profile for t = 1 year ; right: Pressure profile for t = 6 years .

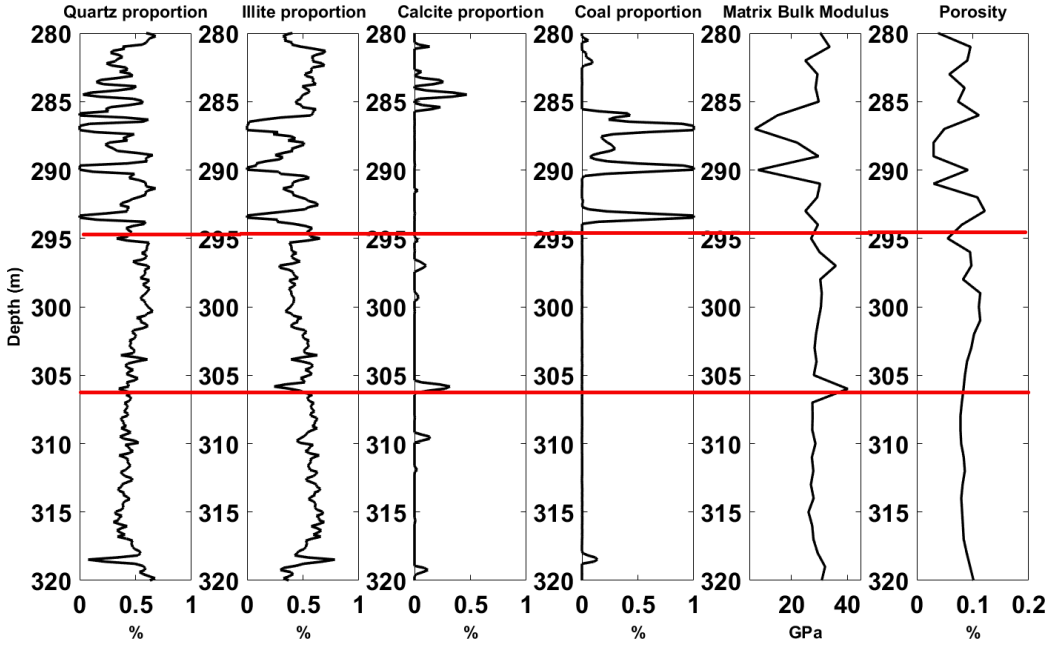

FIG. 5. Mineral composition along the well (ELAN log, Schlumberger) and associated matrix bulk modulus (using K_{quartz} = 36.6 GPa ; K_{illite} 12 GPa ; $K_{calcite}$ = 74 GPa ; K_{coal} = 7 GPa). Reservoir limits for t = 6 years are added in red.

All the different parameters came with different space gridding. All data are rescaled to a final 3D gridding of $5m \times 5m$ horizontally and $1m$ vertically. Final size of the model is $500m \times 500m \times 500m$.

Results

We had detailled data coming from the different wells located at CaMI.FRS. The CO_2 saturation is modelled from the work of Dongas (2016) and Barraza (2016). The combination of those data give us one of the most detailed fluid substitution modelling studies found in the literature.

Results of the Gassmann fluid substitution can be seen on Figure 6. This figure shows 2D sections of the variation of the elastic parameters for t= 6 years (1 year after the end of the injection). The shape of the anomalies is perfectly correlated with the shape of the CO_2 reservoir (Figure 3.b). The mean variations calculated for the 3-D reservoir are summarized in the table 2.

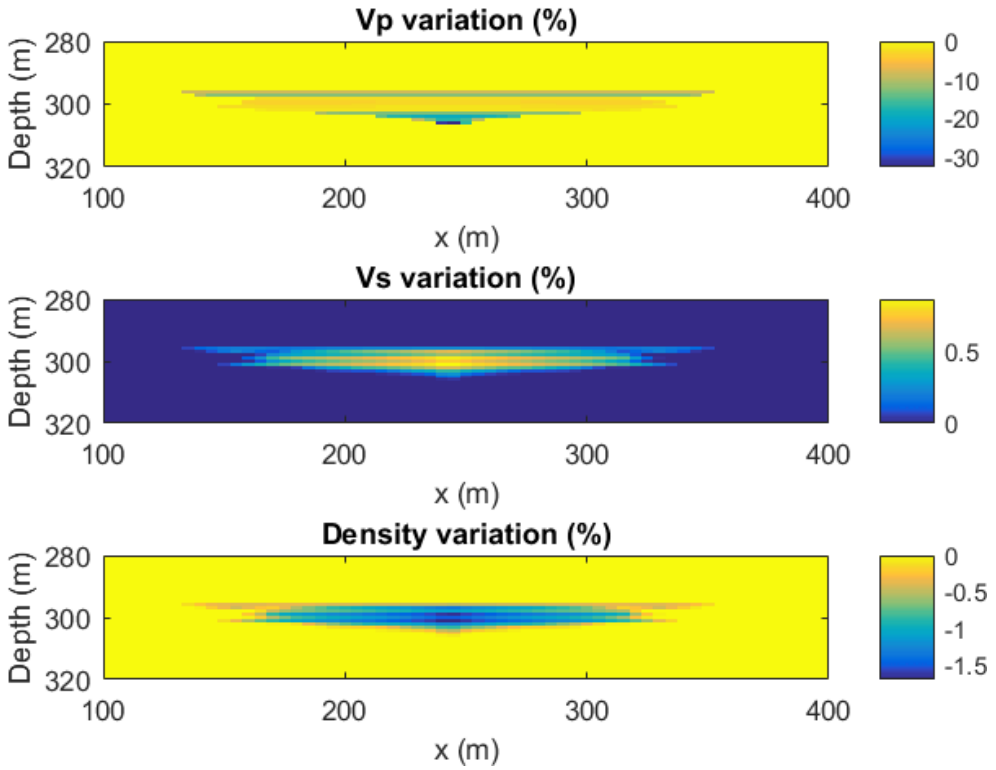

FIG. 6. Top: 2D section of the P-wave velocity variation at t= 6 years, focussed on the CO_2 reservoir injection. Middle: 2D section of the S-wave velocity variation at t= 6 years, focussed on the CO_2 reservoir injection. Bottom: 2D section of the density variation at t= 6 years, focussed on the CO_2 reservoir injection.

Table 2. Mean elastic parameters variations (in $\%$), for the 3-D reservoir.

	V_p	V_S	ρ
t = 1 year (1 year after the beginning of the injection)	-5.03	0.21	-0.41
t = 6 years (1 year after the end of the injection)	-6.25	0.31	-0.61

Figure 7 shows 1D profiles of the variation of different parameters in the injection well. The variation in P-wave velocity can reach up to -20 $\%$, variation in S-wave velocity are around 0.75$\%$ and variation in density are around -1.5$\%$.

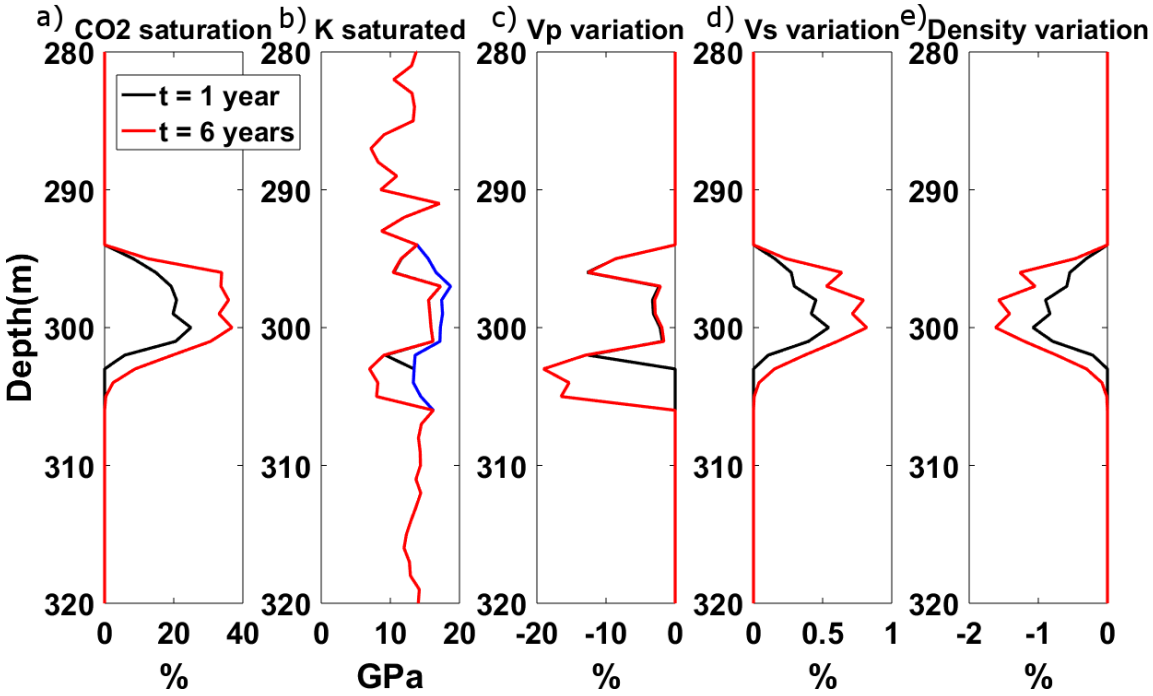

FIG. 7. a) CO_2 saturation 1 year after the end of the injection. b) Saturated bulk modulus in the initial model (before) and 1 year after the end of the injection (after). c) P-wave velocity variation between the initial model and 1 year after the end of the injection. d) S-wave velocity variation between the initial model and 1 year after the end of the injection. e) Density variation between the initial model and 1 year after the end of the injection.

Density. Density has only a small variation and is perfectly correlated with the CO_2 saturation. The new density is computed using the equation 13. In this equation, the only variable which changes is the density of the new fluid. It decreases from 1.002 $g.cc^{-1}$ to 0.69 $g.cc^{-1}$ (Table 1). The bulk rock density decreases linearly with it.

S-wave velocity. The S-wave velocity does not vary a lot between the initial model and the two different time periods. This can be explained by the fact that this parameter is only dependant in changes in the new density (as the shear modulus remains the same regardless of the fluid contained in the medium). As the density does not show big variations, the S-wave velocity does not neither. However, note that the V_S increases with the CO_2 injection, due to small changes in the density.

P-wave velocity. This parameter is the most affected by fluid substitution. Moreover, the variation in V_P is not linearly related to the CO_2 saturation as V_P depends on the new saturated bulk modulus (see equation 14). The saturated bulk modulus is the more variable parameter. It depends on the bulk modulus of the fluid which varies significantly between the initial model and the time results (from 2.14 GPa to 0.013 GPa for t = 6 years, see Table 1). We can note that the new saturated bulk modulus variation for t = 1 year and t = 6 years are quite similar (Figure 7.b). This parameter is only controlled by the new fluid bulk modulus (see equation 12). As the values of the fluid bulk modulus are very close for the two time-lapse models (0.026 Gpa for t = 1 year and 0.013 for t = 6 years), the new

saturated bulk moduli are also very close for the two time-lapses models ; and so the new V_P are also very close for t = 1 year and t = 6 years.

To conclude on the results on fluid substitution, the difference in P-wave velocity is the parameter which will influence the most the results expected to be seen on the seismic data. Nevertheless, the variation in V_P are very close for the two time-lapses models and we can predict that it can be difficult to recover the CO_2 saturation only from V_P.

DATA SIMULATION AND PROCESSING

Seismic data were simulated with Tiger (SINTEF Petroleum Research), a 3D finite-difference modelling software. The advantage of this software is the possibility of parallelization which decreases the computation time, especially useful in a complex 3D velocity model and for a quite big survey.

The survey configuration used is a simplified version of the survey acquired in May 2014 (Isaac and Lawton, 2015), and is shown in Figure 8. We use a Ricker wavelet (dominant frequency $40Hz$) as source. Data were processed with Vista processing software. One of the advantage of working with synthetic data is the simplification of the processing. Even if we compute the 3 components, we only use here the vertical one in this study. A standard processing is applied to the data: deconvolution, Normal Move-Out, CMP stack and finite-difference migration. Due to the survey parameters (see Figure 8), the final bin size is $25m \times 25m$.

a)

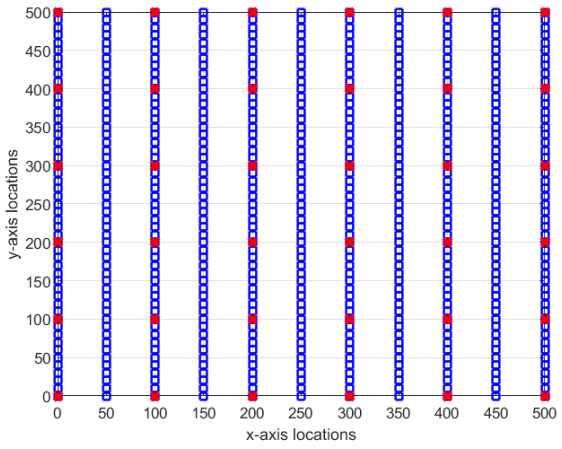

b)

Parameter	Value
Source line interval	50 m
Receiver line interval	100 m
Source spacing	100 m
Receiver spacing	10 m

FIG. 8. Acquisition parameters for seismic simulation. a) Blue squares are receivers ; red crosses are sources. b) Summary table.

Figure 9.a shows vertical slices in the baseline 3D seismic volume. Because it is difficult to visually compare 3D seismic volumes, we usually prefer to show the difference between them. Figures 9.b and 9.c show the difference between the two time-lapse seismic volume and the baseline. We can see in those figures the shape of the expected CO_2 plume in the reservoir.

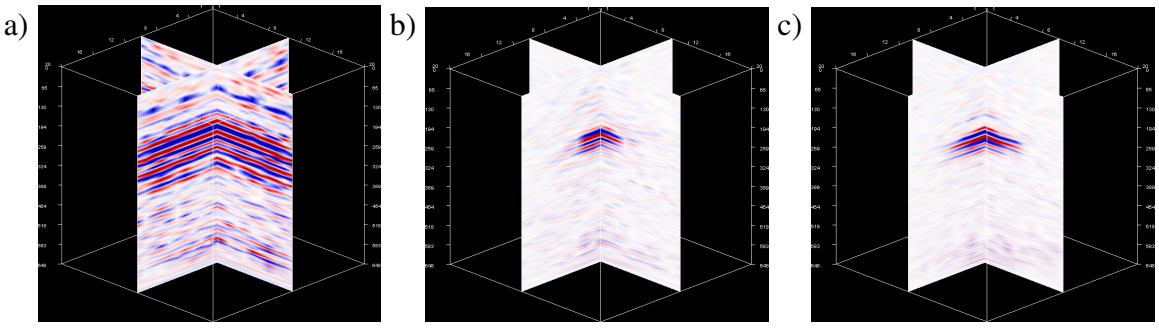

FIG. 9. Results of the processing on the seismic data. a) Baseline 3D volume. b) Monitoring on t = 1 year (3D volume at t = 1 year - baseline 3D volume). c) Monitoring on t = 6 years (3D volume at t = 6 years - baseline 3D volume).

Figure 10 shows 2-D sections extracted from the middle of the 3-D volumes. The section is smoothed (because the bin size is $25m$) but we can see that the lateral expansion of the reflectivity anomaly corresponds well to the lateral dimensions of the CO_2 plume.

We can also see the time-lapse anomaly on the horizontal slices (Figure 11). Those slices are taken at the two-way travel time twt = $0.21s$. Considering a mean velocity of 2800 $m.s^{-1}$ the corresponding depth is $294m$. It corresponds to the depth of the top of the CO_2 reservoir. The contour of the lateral expansion of the CO_2 plume is added as red line. We can see that the anomaly in seismic data is well contained inside this contour. Note that the amplitude is weaker for the time-lapse t = 1 year than for the time-lapse t = 6 years.

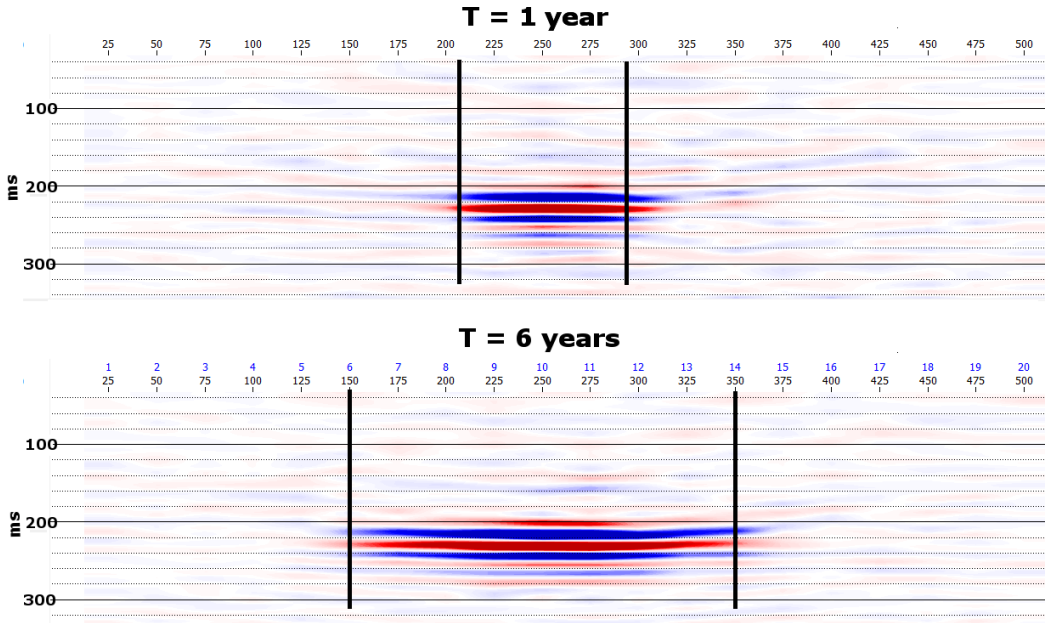

FIG. 10. 2-D sections, Inline = 10 (y=$250m$). Top: for 1 year after the beginning of the injection (t = 1 year) ; bottom: for 1 year after the end of the injection (t = 6 years). On both figure, the lateral extension of the CO_2 plume calculated are added as black lines.

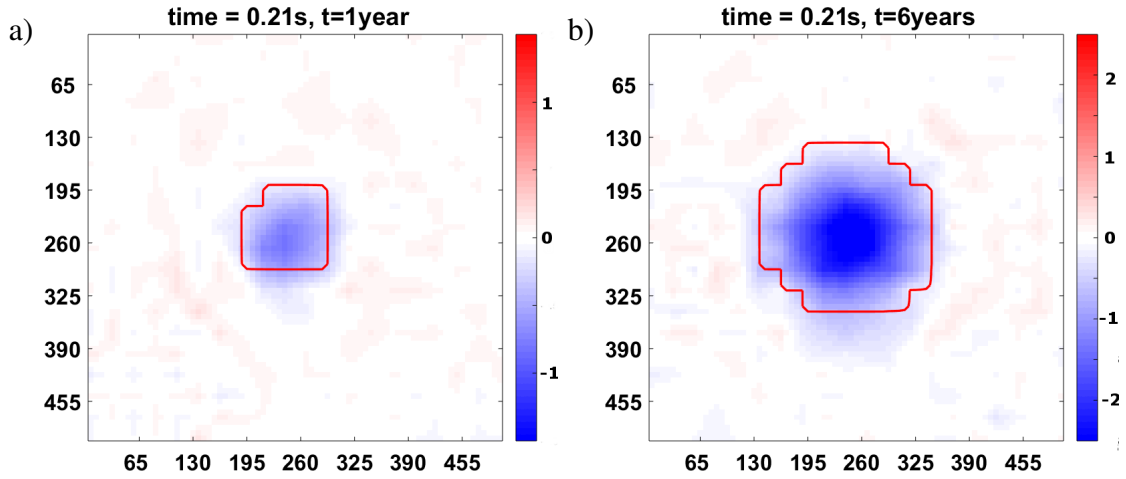

FIG. 11. Horizontal sections at two-way travel time twt = 0.21s. a) For 1 year after the beginning of the injection. b) For 1 year after the end of the injection. Expected lateral expansion of the CO_2 plume is added as red line.

WORK IN PROGRESS

From the seismic data, we see that we are able to recover the size of the CO_2 plume. It is one of the main objective of the monitoring: be able to image the plume, be able to track the CO_2 migration and be able to detect any leakage. Nevertheless, one can ask if we are able to recover the saturation of CO_2 in the reservoir. One way is to study the amplitude of the seismic signal and try to relate it to the gas saturation. One other way can be to recover the elastic parameters (V_P, V_S and ρ) and try to use them directly to recover the gas saturation.

We use the well-tying method (Lloyd and Margrave (2013)) and the bandlimited impedance inversion algorithm developed by Ferguson and Margrave (1996) to recover the P-impedance in the three different models (baseline, t = 1 year and t = 6 years).

Figure 12 shows the real P-impedance smoothed (in black) and the inverted P-impedance (in red) for the different time-lapses, converted in depth. The difference between the real and the inverted P-impedance is due to the process of the inversion, as the estimation of the wavelet for instance. Nevertheless, the general trend is recovered well.

Figure 13 shows the variation in impedance between the time-lapse survey and the baseline. Black curves show the result for the real impedance (smoothed) and red curves shows the results for the inverted impedance. Because of the resolution of the seismic data ($25m$ x $25m$), we average the real impedance variation over this same distance. It explains why the real impedance inversion shows a smoother curve than in Figure 7.

Even from this initial work, the impedance inversion is able to recover the variation in P-impedance induced by the fluid substitution. Figure 13 shows that we recover the same variation in impedance than the one we expected (around 3% for t = 1 year and around 7.5% for t = 6 years at $300m$ depth). The unexpected variation of impedance observed on the inverted data are due to the inversion process, probably due to the estimation of the wavelet.

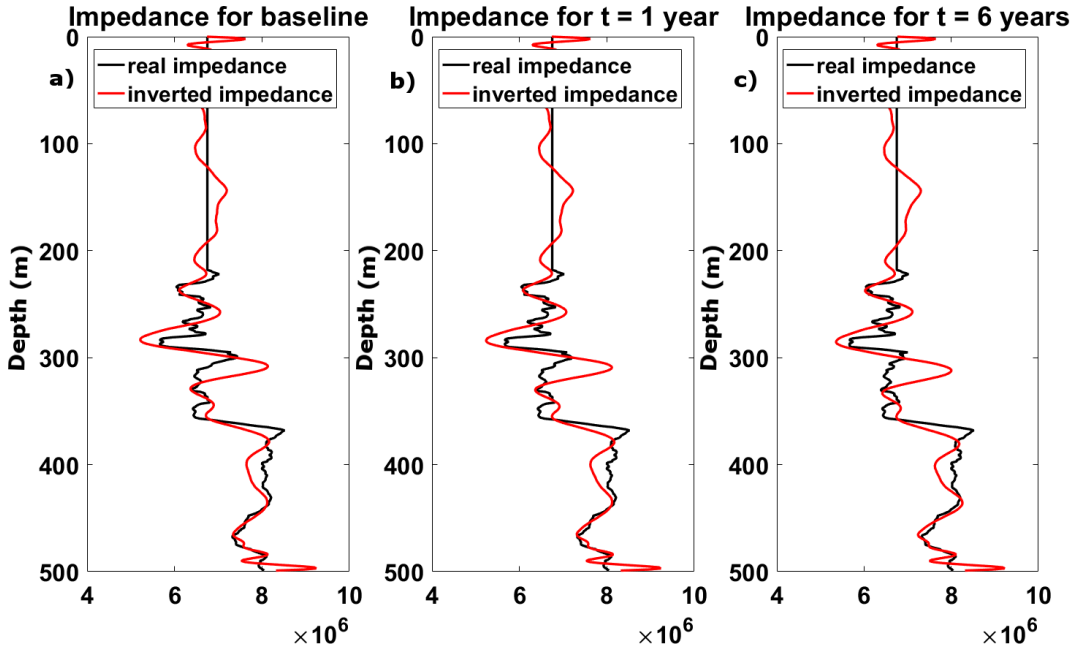

FIG. 12. Real (black) and inverted P-impedance (red) for a) the baseline ; b) 1 year after the beginning of the injection (t = 1 year) and c) 1 year after the end of the injection (t = 6 years).

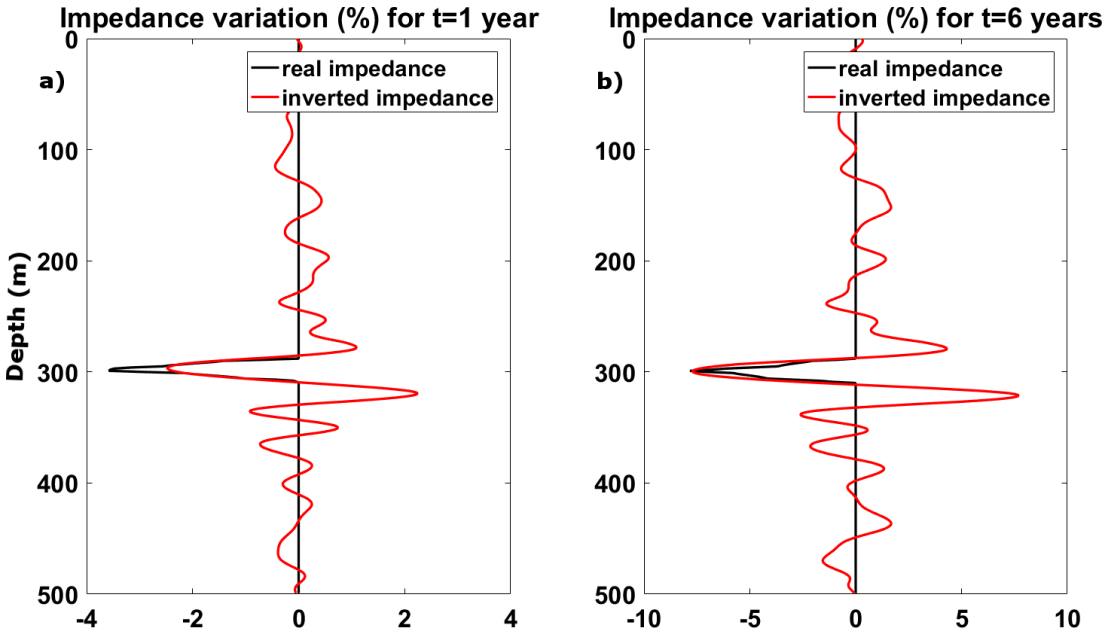

FIG. 13. Variation in impedance. a) Between the baseline and monitor t = 1 year. b) Between the baseline and monitor t = 6 years. In black: for the real impedance ; in red: for the inverted impedance.

CONCLUSIONS AND FUTURE WORK

The main goal of this work was to qualify the feasibility of time-lapse seismic monitoring of CO_2 sequestration on a small and shallow reservoir. Accurate input data and Gassmann fluid substitution gave us the possibility to produce accurate elastic parameters (V_P, V_S and ρ) models before injection (baseline) and for different time-lapse surveys (here 1 year after the beginning of the injection and 1 year after the end of the injection). Seismic data are generated in this model and processed to give us three 3D seismic volumes. The difference between the time-lapse volume and the baseline volume recovers the shape of the CO_2 plume in the reservoir. The work on the impedance inversion shows that we are able to recover the variation in P-impedance induced by fluid substitution using those seismic data.

Because of computation time and the choice of our survey parameters, the spatial resolution of our data is quite poor compared to what we are able to obtain with a field survey. However, as the shape of the reservoir and the variation in P-impedance are well recovered, we can easily confirm that it would be the same even with higher density surveys.

For future work, we propose to study PS seismic data. Indeed, we also simulated the horizontal component responses. We need to process the data and invert them for S-impedance.

We recently simulated the data using a different 2D survey configuration, which include down-hole receivers. This new configuration should allow a better spatial resolution in the seismic data, and should also improve the spatial resolution in the impedance inversion.

ACKNOWLEDGEMENTS

We thank CMC and the CREWES sponsors for their financial support. We also gratefully acknowledge support from NSERC (Natural Science and Engineering Research Council of Canada) through the grant CRDPJ 461179-13. We also thank SINTEF for providing access to the TIGER modelling software.

REFERENCES

Barraza, J., 2016, Static model - geomodel upgraded: PPT Presentation - CMC Research Institutes, Inc.

Batzle, M., and Wang, W., 1992, Seismic properties of pore fluids: Geophysics, **57**, No. 11, 1396–1408.

Dongas, J. M., 2016, Development and characterization of a geostatic model for monitoring shallow CO2 injection: Master Thesis, University of Calgary.

Ferguson, R. J., and Margrave, G. F., 1996, A simple algorithm for bandlimited impedance inversion: CREWES Research Report, **8**.

Gassmann, F., 1951, Uber die elastizität poröser medien: Vierteljahrsschrift der naturforschenden Gesellschaft in Zürich, **96**, 1–23.

Gassmann, F., 1998, On elasticity of porous media: Vierteljahrsschrift der naturforschenden Gesellschaft in Zürich.

Hall, K. W., Isaac, J. H., Wong, J., Bertram, K. L., Bertram, M. B., Lawton, D. C., Bao, X., and Eaton, D., 2015, Initial 3C-2D surface seismic and walkaway VSP results from the 2015 Brooks SuperCable experiment: CREWES Research Report, **27**.

Isaac, J. H., and Lawton, D. C., 2015, 3D3C seismic data at the Brooks experimental CO2 injection site: CREWES Research Report, **27**.

Lawton, D. C., Bertram, M., Bertram, K., Hall, K., and Isaac, H., 2015a, A 3C-3D seismic survey at a new field research station near Brooks, Alberta: CREWES Research Report, **27**.

Lawton, D. C., Bertram, M., and Bertram, K. H. K., 2015b, New approaches to seismic monitoring at the Brooks Field Research Station: CREWES Research Report, **27**.

Lloyd, H. J. E., and Margrave, G. F., 2013, The art of well tying with new MATLAB tools: CREWES Research Report, **25**.